

Article

Preparation and Characterization of Nano-Sized Co(II), Cu(II), Mn(II) and Ni(II) Coordination PAA/Alginate Biopolymers and Study of Their Biological and Anticancer Performance

Maged S. Al-Fakeh ^{1,2,*} , Munirah S. Alazmi ¹ and Yassine EL-Ghoul ^{1,3}

¹ Department of Chemistry, College of Science, Qassim University, Buraidah 51452, Saudi Arabia; m-alazmi@qu.edu.sa (M.S.A.); y-elghoul@qu.edu.sa (Y.E.-G.)

² Taiz University, Taiz 3086, Yemen

³ Textile Engineering Laboratory, University of Monastir, Monastir 5019, Tunisia

* Correspondence: m.alfakeh@qu.edu.sa

Abstract: Four of the crosslinked sodium alginate and polyacrylic acid biopolymers based nanoscale metal natural polysaccharides, $[M(AG-PAA)Cl(H_2O)_3]$, where $M = Co(II), Cu(II), Mn(II)$ and $Ni(II)$, AG = sodium alginate and PAA = polyacrylic acid, have been synthesized and structurally characterized. Because of their numerous biological and pharmacological activities of polysaccharides, including antimicrobial, immunomodulatory, antitumor, antidiabetic, antiviral, antioxidant, hypoglycemic and anticoagulant activities, polysaccharides are one of the near-promising candidates in the biomedical and pharmaceutical fields. The complexity of the polymeric compounds has been verified by carbon and nitrogen analysis, magnetic and conductance measurements, FT-IR spectra, electronic spectral analysis and thermal analysis (DTA, TG). All the synthesized complexes were non-electrolytes with magnetic moments ranging from 1.74 to 5.94 BM. The polymeric complexes were found to be of octahedral geometry. The developed coordination polymeric was found to be crystalline using X-ray powder diffraction examinations, which is confirmed by the SEM analysis. As a result, the crystallite size of all polymeric nanocrystals was in the range of 14 - 69 nm. The test of four compounds exhibits a broad spectrum of antimicrobial activity against both Gram-positive and Gram-negative bacteria and fungal *Candida albicans*. Using DPPH as a substrate, studies on radical scavenging tests are carried out. The findings demonstrated the antioxidant activities of each complex. In addition, results showed that the two chosen polymeric complexes had a good ability to kill cancer cells in a dose-dependent way. The copper(II) polymeric complex showed to its superior functionality as evidenced by microbial activity. After 72 h of interaction with the normal human breast epithelial cells (MCF10A), the synthesized polymeric compounds of Cu(II) and Co(II) showed exceptional cytocompatibility with the different applied doses. Compared to poly-AG/PAA/Co(II), poly-AG/PAA/Cu(II) exhibits a greater anticancer potential at various polymeric dosages.

Keywords: crosslinked sodium alginate and polyacrylic acid biopolymers; XRD; scanning electron microscopy; antimicrobial activity; antioxidants and anticancer



Citation: Al-Fakeh, M.S.; Alazmi, M.S.; EL-Ghoul, Y. Preparation and Characterization of Nano-Sized Co(II), Cu(II), Mn(II) and Ni(II) Coordination PAA/Alginate Biopolymers and Study of Their Biological and Anticancer Performance. *Crystals* **2023**, *13*, 1148. <https://doi.org/10.3390/cryst13071148>

Academic Editor: Waldemar Maniukiewicz

Received: 19 June 2023

Revised: 14 July 2023

Accepted: 21 July 2023

Published: 23 July 2023



Copyright: © 2023 by the authors. Licensee MDPI, Basel, Switzerland. This article is an open access article distributed under the terms and conditions of the Creative Commons Attribution (CC BY) license (<https://creativecommons.org/licenses/by/4.0/>).

1. Introduction

As biopolymers (BPs) are composed of living organisms such as microbes and plants, they are a renewable materials resource, unlike most polymers which are petroleum-based coordination polymers. Generally, biopolymeric complexes are degradable. They find use in different industries from food industries to packaging, manufacturing and biomedical engineering [1–3]. BPs are heartening materials owing to their properties such as biocompatibility, unique properties and abundance such as non-toxicity, etc. With some nano-sized reinforcements to promote their characteristics and experimental applications, BPs are being researched for their use in more and more methods possible. Biopolymer compounds are divided into four main categories: those made from microorganisms, biomass products

(agro-biopolymers), biotechnological products and petrochemical products [4]. Numerous different substances, including polysaccharides (starches, celluloses, alginates, pectin's, gums and chitosan), are found in biopolymers made from biomass products [5–8]. Other applications of biopolymers are used in the production of nanomaterials. Nanotechnology, also known as 1 nm to 100 nm scale manipulation, is the process of changing the size and shape of structures, systems and electronics [9–11]. Due to their small size, they have higher reactivity than the corresponding bulk forms, more significant surface areas and a variety of properties that can be tuned [12–14]. These unique characteristics have accelerated the development of nanoscience and the use of nanoparticles in a diversity of industries, including cosmetics, electronics, food analysis, the environment, biomedicine and other applications [15–19]. Important characteristics of biopolymers include their biodegradability, biocompatibility, stability, sustainability, bioresorbability, flexibility, renewability and antibacterial and antifungal activity [20–24]. They are also less toxic, non-immunogenic, easier to extract, carbon-neutral, non-carcinogenic and non-thrombogenic [25–27]. Because of the numerous biological and pharmacological activities of polysaccharides, including antitumor, antioxidant, anticoagulant, immunomodulatory, antimicrobial, hypoglycemia activities, antidiabetic and antiviral activities, polysaccharides are one of the maximally promising candidates in pharmaceutical and biomedical applications. Polysaccharides (PSD) are fundamental macromolecules that nearly exist in all living forms and have significant biological functions. There are numerous sources of polysaccharides, including plants, microorganisms, algae and animals [28,29]. Alginates are a type of polysaccharide that is primarily derived from brown algae and bacteria found in seaweed. This bio-material is a naturally occurring polysaccharide that also occurs as capsular (PSD) in some bacteria, for example, *Azotobacter* and *Pseudomonas*, and as structural elements in the cell walls of marine brown algae such as *Phaeophyceae*. Alginates (AGs) constitute a strain of linear binary unbranched co-polymers consisting of α -L-guluronic acid (monomer G) and 1,4-linked β -D-mannuronic acid (monomer M) residues. Sodium alginate (Na-AG) is the sodium salt composed of alginic acid and gum mainly extracted by the cell walls of brown algae, with chelating activity (Figure 1) [30,31]. AGs, natural multifunctional polymers, have gained prominence as desirable compounds in pharmaceutical industries and biomedicine over the past few decades as a result of their distinctive physicochemical characteristics and diverse biological activities [32,33]. They are non-antigenic, biocompatible, non-toxic and biodegradable [34,35]. Additionally, alginates are used in food manufacturing as a gelling, thickening, stabilizing or emulsifying agent, as a by-product of microbial and viral protection and to coat fruits and vegetables, whereas alginate substantially contributes to the sustained release of drug-delivery products [36].

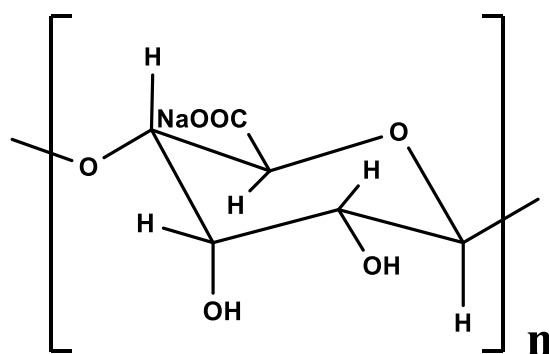


Figure 1. Chemical structure of sodium alginate (Na-AG).

Polyacrylic acid (PAA) is the most basic acrylate polymer [37]. The structure of (PAA), which has a carbon backbone and an ionizable COOH group as a side chain in each reiterates unit, is depicted in (Figure 2). In water with a pH of 7, (PAA) is an anionic polymer, meaning that many of its COOH groups will lose their H^+ and develop a negative charge.

As a polyelectrolyte, PAA can therefore absorb and hold onto water, expanding to many times its initial volume [38]. In recent years, interest in PAA, a non-toxic, biodegradable and biocompatible polymer, has increased significantly. By chemically altering carboxyl groups, it is possible to create PAA nano-derivatives, which have better chemical properties than unaltered PAA [39]. An acrylic acid (AA), polymer with a (-COOH) on each of monomer unit end is known as PAA, also referred to as a carbomer. PAA, a thermoplastic polymer, has a high bioavailability due to its numerous carboxyl groups, thus serving as a surface variation for biological nano-materials [40]. Cross-linked PAA has also been used in the processing of household products, inclusively floor cleaners. The neutralized (PAA) gels are appropriate to obtain biocompatible matrices used for medical applications, for example, gels for skin disease treatment products or skin care [41].

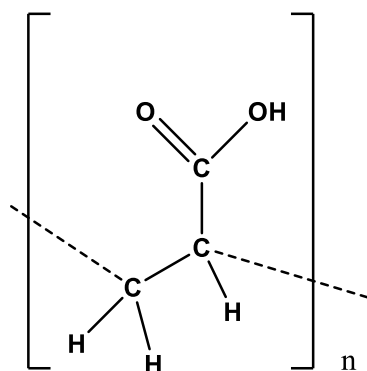


Figure 2. Chemical structure of polyacrylic acid (PAA).

Previously, Ni(II) and Co(II) alginate biopolymer complexes and polyacrylic acid nanoplateforms were reported to show antimicrobial, anticancer and biosensing [42,43]. Therefore, we meditate that polymeric compounds of nano-sized Co(II), Cu(II), Mn(II) and Ni(II)-PAA/alginate biopolymers will show more antioxidant, antibacterial and anticancer activity. In light of these results, we created a work on metal-PAA/alginate biopolymers compounds, which included a review of their NPs and testing for antifungal, antibacterial, antioxidative and anticancer properties. The primary goal of this paper is to synthesize and analyze the physicochemical properties of nanoscale polymeric complexes of cobalt(II), copper(II), manganese(II) and nickel(II) that have been synthesized in both the solid and solution states. CHN, UV-vis, FT-IR, spectra, molar conductance, magnetic, TG, DTA, XRD and scanning electron microscopy are used to depict the framework of the examined compounds. Further, the metal polymeric coordination compounds' antibacterial, antifungal and antioxidant characteristics as well as their anticancer research are presented.

2. Materials and Methods

The chemicals listed below were analytical-grade substances that were used directly after delivery without further purification. Sodium Alginate, poly-(acrylic acid), methanol, dimethyl sulfoxide (DMSO), Co(II) chloride hexahydrate, Cu(II) chloride dehydrate, Mn(II) chloride tetrahydrate and Ni(II) chloride hexahydrate were all purchased from Sigma-Aldrich company.

2.1. Preparation of the Crosslinked Polymeric Ligand (Poly-PAA/AG)

First, we vigorously stirred 100 mL of distilled water with 3 g of sodium alginate (AG) for an hour at 80 °C in a round bottom flask. Then, we added dropwise a polyacrylic acid (PAA) solution that had been previously made by combining 3 g of PAA with 100 mL of H₂O, stirring continuously and heating at 70 °C. Under N₂ pressure, the mixture was stirred at 120 °C for two hours. The reaction solution was then preserved at 90 °C overnight while being stirred. The resultant suspension was then brought to 25 °C before being concentrated at a lower pressure. The final step was to dry the obtained product at 65 °C

while maintaining a high vacuum, producing a white color stable powder (90%). Anal. Calc. for $C_9H_{10}O_7$: C, 46.97; H, 4.38. Found: C, 46.93; H, 4.98. IR data: $\nu_{(OH)}$ 3222, $\nu_{(C-H)}$ 2922, $\nu_{(C=O)}$ 1725, $\nu_{(COO)}$ 1413, $\nu_{(CO)}$ 1263, $\nu_{(C-O-C)}$ 1025.

2.2. Synthesis of Metal Polymeric Complexes Nanoparticles

2.2.1. $[Co(AG-PAA)Cl(H_2O)_3]$

This compound was made by dissolving 1 g (0.2 mmol) of the (AG/PAA) ligand in 20 mL of methanol, boiling it for 5 min and then stirring while adding 20 mL of pure water until the ligand dispersed. We allowed the mixture to cool somewhat before adding 0.82 g (0.2 mmol) of the metal ($CoCl_2 \cdot 6H_2O$), which had been dissolved in 10 mL of distilled water. Stirring continuously until the purple precipitate forms, it is then dried over $CaCl_2$ in a desiccator. Anal. Calc. for $C_9H_{15}CoClO_{10}$: C, 28.62; H, 4.00. Found: C, 29.06; H, 4.28. IR data: $\nu_{(OH)}$ 3225, $\nu_{(C-H)}$ 2930, $\nu_{(COO)_{sym}}$ 1715, $\nu_{(C=O)}$ 1715, $\nu_{(COO)_{asym}}$ 1415, $\nu_{(CO)}$ 1157, $\nu_{(C-O-C)}$ 1022, $\nu_{(M-O)}$ 519 cm^{-1} , m.p. 230 °C and molar conductance 18.63 $S\ cm^2\ mol^{-1}$.

2.2.2. $[Cu(AG-PAA)Cl(H_2O)_3]$

This complex was prepared by dissolving 0.5 g (0.1 mmol) of the (AG/PAA) ligand in 20 mL of methanol and heating it for 5 min before adding 20 mL of distilled water and heating and stirring until the ligand was dissolved. We allowed it to cool somewhat before adding 0.37 g (0.1 mmol) of the metal salt ($CuCl_2 \cdot 2H_2O$) that was dissolved in 10 mL of distilled water. The resultant mixture was stirred, and then the mixture solution containing copper(II) complex was sonicated for 30 min; then, the green polycrystalline powder was obtained, filtered and then cooled to room temperature. The green precipitate was washed with distilled water and ethanol and then dried over $CaCl_2$ in a desiccator. Anal. Calc. for $C_9H_{15}CuClO_{10}$: C, 28.28; H, 3.95. Found: C, 28.61; H, 3.98. IR data: $\nu_{(OH)}$ 3199, $\nu_{(C-H)}$ 2932, $\nu_{(COO)_{sym}}$ 1703, $\nu_{(C=O)}$ 1703, $\nu_{(COO)_{asym}}$ 1421, $\nu_{(CO)}$ 1273, $\nu_{(C-O-C)}$ 1026, $\nu_{(M-O)}$ 582 cm^{-1} , m.p. 190 °C and molar conductance 17.85 $S\ cm^2\ mol^{-1}$.

2.2.3. $[Mn(AG-PAA)Cl(H_2O)_3]$

This compound was synthesized in 2 steps:

Step 1: In a beaker, 0.8 g (0.2 mmol) of AG-PAA was dissolved in 20 mL of methanol, and the mixture was heated for five minutes. Next, 20 mL of distilled water was added, and the mixture was stirred and heated for another 20 min.

Step 2: We added the metal solution (0.68 g, 0.2 mmol) of tetra-hydrated manganese chloride, which was dissolved in 10 mL of distilled water. After allowing it to cool down a bit, we stirred it until the light brown precipitate formed and then dried it in calcium chloride anhydrous. Anal. Calc. for $C_9H_{15}MnClO_{10}$: C, 28.93; H, 4.04. Found: C, 29.10; H, 4.47. IR data: $\nu_{(OH)}$ 3444, $\nu_{(C-H)}$ 2931, $\nu_{(COO)_{sym}}$ 1696, $\nu_{(C=O)}$ 1696, $\nu_{(COO)_{asym}}$ 1419, $\nu_{(CO)}$ 1103, $\nu_{(C-O-C)}$ 1027, $\nu_{(M-O)}$ 523 cm^{-1} , m.p. 210 °C and molar conductance 14.18 $S\ cm^2\ mol^{-1}$.

2.2.4. $[Ni(AG-PAA)Cl(H_2O)_3]$

The 0.8 g of the (AG/PAA) ligand was dissolved in 20 mL of methanol, heated for 5 min, and stirred until the ligand was dissolved. Next, 20 mL of distilled H_2O was added, and the mixture was heated and stirred for an additional minute. We allowed it to cool slightly before adding 0.65 g of the metal ($NiCl_2 \cdot 6H_2O$), which was dissolved in 10 mL of distilled H_2O . We continued stirring until the light green precipitate forms, after which it is dried in the calcium chloride anhydrous. Anal. Calc. for $C_9H_{15}NiClO_{10}$: C, 28.64; H, 4.00. Found: C, 28.92; H, 4.33. IR data: $\nu_{(OH)}$ 3216, $\nu_{(C-H)}$ 2925, $\nu_{(COO)_{sym}}$ 1700, $\nu_{(C=O)}$ 1700, $\nu_{(COO)_{asym}}$ 1414, $\nu_{(CO)}$ 1164, $\nu_{(C-O-C)}$ 1018, $\nu_{(M-O)}$ 515 cm^{-1} , m.p. 196 °C and molar conductance 19.15 $S\ cm^2\ mol^{-1}$.

2.3. Physical Measurements

A Gmbh Vario El analyzer was used to determine the elemental analyzers. A Thermo Nicolet (6700), Fourier-transform infrared (FT-IR) spectrophotometer with a wavenumber range of (400–4000 cm^{-1}) was used to collect structural data from FT-IR spectra. Using a Shimadzu (UV-2101) PC spectrophotometer, the UV-Vis spectra were collected. The sonication experiments were performed on sonicator type Q 700, 20 KHz, output 700 W. On a magnetic susceptibility balance of the kind (MSB-Auto), measurements of magnetic susceptibility were made. Using a conductivity meter made by JENWAY, model 4310, the complexes' conductance was measured. On a Shimadzu (DTG 60-H) thermal analyzer heated to a rate of 10 $^{\circ}\text{C}$ per minute, thermal analysis of the polymeric complexes was performed in dynamic air. On an XRD diffractometer Model (PW 1720 Philips, Eindhoven, The Netherlands), measurements of the X-ray diffraction (XRD) were collected at room temperature with Cu-K α radiation ($\lambda_{\text{Cu}} = 0.154059 \text{ \AA}$). In the structural refinement procedure of our samples, we have followed the standard steps of the Rietveld method which consists of following the sequence:

- (i) Refinement of overall Scale factor + background coefficients (all other parameters are kept fixed);
- (ii) The same + refinement of detector zero offsets (or sample displacement in Bragg-Brentano geometry) + refinement of lattice parameters;
- (iii) The same + refinement of shape parameters + refinement of asymmetry parameters;
- (iv) The same + refinement of atomic positions + refinement of global DebyeWaller parameter or thermal agitation factors;
- (v) The same + refinement of site occupancy rate. In our refinements, we have taken care to respect this sequence of steps to release the different parameters. This ensures the stability of the refinement with all the parameters released.

By computing indicators such as the goodness of fit " χ^2 " and the R factors (R_{wp} = weighted profile R-factor, R_{B} = Bragg factor and R_{exp} = expected R factor), the fitting quality of the experimental data is evaluated.

Using a scanning electron microscope, the morphology and structure of the prepared materials were examined.

2.4. Microbial Species and Culture Media

In this article, various metal polymeric complexes, such as Co(II), Cu(II), Mn(II) and Ni(II), were tested against Gram-positive (+) and Gram-negative (−) bacterial strains to gain insight into their broad-spectrum effect. Two Gram-positive strains, *Micrococcus luteus* NCIMB 8166 (S4) and *Staphylococcus aureus* ATCC 25923 (S1), and two Gram-negative strains, *Salmonella thyphimurium* ATCC 14028(S10) and *Escherichia coli* ATCC 35218 (S5), were the pathogenic strains that were used. A pathogenic reference strain of the yeast *Candida albicans* ATCC 90028 (9C) was used to test the antifungal activity. The strains were cultured on nutrient agar (Oxoid) for 24 h at 37 $^{\circ}\text{C}$ as well as in nutrient broth (Oxoid) for 24 h at 37 $^{\circ}\text{C}$. For 24 h, the yeast strain was grown at 25 $^{\circ}\text{C}$ in Sabouraud Chloramphenicol broth (Oxoid) and grown for 24 h at 37 $^{\circ}\text{C}$ on Sabouraud Chloramphenicol agar (Oxoid). The different species are listed in Table 1.

Table 1. The used microbial strains.

Microbe Type	Strain	Reference
Gram-positive bacteria	S1	<i>Staphylococcus aureus</i> ATCC 25923
	S4	<i>Micrococcus luteus</i> NCIMB 8166
Gram-negative bacteria	S5	<i>Escherichia coli</i> ATCC 35218
	S10	<i>Salmonella thyphimurium</i> ATCC 14028
Yeast	9C	<i>Candida albicans</i> ATCC 90028

2.5. Antimicrobial Activity

All complexes were tested for antimicrobial activity using the agar disk diffusion method. A total of 50 mg of each extract was dissolved in 1 mL of a 5% solution of dimethyl sulfoxide, or “DMSO,” prior to testing. The strains were cultured in Mueller–Hinton (MH) broth (Oxoid) at 37 °C for 24 h, and suspensions were calibrated to 0.5 McFarland standard turbidity. Afterward, 100 µL of each precultured suspension was spread onto plates containing MH agar. Sterile filter paper discs (6 mm in diameter) were impregnated with 20 µL of the different extracts and placed on agar. The treated plates were put for 1 h at 4 °C and then incubated for 24 h at 37 °C. After incubation, the diameter of the inhibition zone (clear halo) about the discs was measured. Each sample was tested in duplicate.

2.6. Antioxidant Assays

DPPH Radical Scavenging Assay

According to the method proposed by Mahdhi et al. [44], the free radical scavenging influence of the extracts was assessed using the next criteria: 1 mL of sample (5 mg/mL) was combined with 3 mL of DPPH (2,2-diphenyl-1-picrylhydrazyl) (300 µM) methanolic solution. The reaction mixture was vortexed and left to sit at 25 °C for 30 min. The solution’s absorbance was determined at 517 nm. The standard was ascorbic acid. The following Equation (1) was used to determine the inhibitory % of DPPH:

$$\text{DPPH Scavenging effect (\%)} = [1 - (\text{Abs sample}/\text{Abs control})] \times 100 \quad (1)$$

2.7. Cell Viability and Anticancer Assays

For the cell culture, human breast cancer cells (MCF-7) and human normal breast epithelial cells (MCF-10A) were obtained from American Type Culture Collection (Manassas, WV, USA). The cells were grown in Dulbecco Modified Eagle’s Medium with the addition of a synthesized solution of fetal bovine serum (10%) and a mixture of penicillin (100 IU/mL) and streptomycin (100 g/mL) as antibiotics. The medium was then incubated in a 5% CO₂ atmosphere, 100% relative humidity at 37 °C. The anticancer activity and the cell viability assays were performed via the MTT tetrazolium standardized test with some modifications. This test is based on the ability of live cells to proliferate and thus metabolize and reduce the yellow MTT tetrazolium salt into purple formazan structured by a typical absorbance at 570 nm. The cultivated cells were seeded into 96-well plates at a density of 2104 cells/well. After 24 h of incubation, samples with different concentrations were added to each cell culture medium. After incubation for 72 h, we proceed with the MTT assay. Cell viability was assessed as the average % of relative formazan crystals formed taking into account the control culture. Tests were carried out in triplicate for each test.

3. Results and Discussion

The biopolymers were synthesized by the reaction of AG-PAA with Co(II), Cu(II), Mn(II) and Ni(II) chlorides (dissolved in MeOH and distilled water). The prepared compounds were found to react in the molar ratio of 1: 1: metal: AG-PAA. The polymeric complexes are air-stable and partially soluble in dimethyl sulphoxide. The electrical conductivity of the polymeric compounds adequately confirmed their non-electrolytic nature.

3.1. Elemental Analyses

The results of elemental analyses (carbon and hydrogen) of the ligand and its polymeric complexes along with the proposed molecular formula and physical characteristics were shown in the experimental section.

3.2. Molar Conductance

The molar conductivity of the polymeric complexes was measured in dimethylsulphoxide at 25 °C using 10^{−3} M solutions of polymeric compounds. All complexes had low conductivity readings, proving that they were nonionic, according to the results in Table 2.

Table 2. FTIR spectral bands and their assignments of the ligand and its metal complexes.

Compound	$\nu(\text{O-H})$	$\nu(\text{C-H})$	$\nu(\text{COO})_{\text{sym}}$	$\nu(\text{COO})_{\text{asym}}$	$\nu\Delta$	$\nu(\text{C=C})$	$\nu(\text{CO})$	$\nu(\text{C-O-C})$	$\nu(\text{M-O})$	$\nu(\text{M-Cl})$
AG-PAA	3222	2922	1725	1413	312	1600	1263	1025	-	-
Co(II) complex	3225	2930	1715	1415	300	1599	1157	1022	519	417
Cu(II) complex	3199	2932	1703	1421	282	1592	1273	1026	582	471
Mn(II) complex	3444	2931	1696	1419	277	1595	1103	1027	523	409
Ni(II) complex	3216	2925	1700	1414	286	1604	1164	1018	515	422

$\nu(\text{C=O})$ represents the frequencies of the ester carbonyl obtained after condensation of the AG and the PAA.

3.3. Fourier Transform Infrared Spectra

In order to pinpoint the functional groups of the components and comprehend the binding process, FT-IR spectrophotometric analysis was carried out. In this case, IR analysis was conducted to evaluate the preparation of the polymeric ligand (poly-PAA/AG) via the crosslinking process. However, this method would be crucial in establishing the existence of the various compounds between the created coordination polymer and the several metals examined in our study. Figure 3 displays the various spectra that were obtained. In relation to the synthesis of the polymeric ligand, we observe the appearance of a new band at about 1413 cm^{-1} indicating the fashioning of the ester group when comparing the spectra of the ligand and the alginate or polyacrylic acid biopolymer. This ester fashioning was between the COOH groups of the PAA polycarboxylic acid and the OH groups of the glycosidic moiety of the (AG) biopolymer. Therefore, we conclude that the polymeric ligand (poly-PAA/AG) was obtained through a poly-esterification reaction between the alginate(AG) and the PAA crosslinking agent. The FT-IR spectrum of the (poly-PAA/AG) ligand showed several characteristic bands also existent in the spectra of the initial coordination polymers. Here, we notice the presence of a large band thereabout at 3222 cm^{-1} which is referred to as the hydroxyl group stretching (O-H). The (C-O-C) stretching vibration of the glycosidic structure was visible in a strong band near 1025 cm^{-1} [45]. The pyranose's C-O-C glycosidic bonds are attributed to absorption bands with a wavelength between 1000 and 1100 cm^{-1} . We observe some apparent shifts in the spectra of the compounds when compared to the polymeric ligand (poly-PAA/AG) alone, particularly at 3222 cm^{-1} (O-H), which suggests that the hydroxyl groups of the AG and the various metals have a coordinating binding (Table 2). Furthermore, for $\nu(\text{COO})_{\text{sym}}$ at about 1413 cm^{-1} and $\nu(\text{COO})_{\text{asym}}$ at around 1600 cm^{-1} , we notice clear varied shifts with the used metal revealing the existence of interaction bounds between the different carboxylates of the AG and the various transition elements. In addition, at these wavenumber frequencies, the IR spectra of the complexes showed separation values $\Delta\nu$ (representing the difference between $\nu(\text{COO})_{\text{asym}}$ and $\nu(\text{COO})_{\text{sym}}$) which are around $277\text{--}312\text{ cm}^{-1}$, pointing to a monodentate mode of coordination for the carboxylate group in a network of hydrogen bonds [46]. The IR spectra of the polymeric complexes show a band at $409\text{--}471\text{ cm}^{-1}$ allocated to (M-Cl) [47]. The weak bands at $409\text{--}471\text{ cm}^{-1}$ in the far IR regions were observed for complexes and are attributed to chloride anions coordinated in a trans-octahedral geometry. The existence of coordinated M-O is assured by the band at $515\text{--}582\text{ cm}^{-1}$ that appears with the four complexes [48]. We can deduce that the various functional groups of the prepared crosslinked coordination polymer, the poly-PAA/AG, which is mainly hydroxyl (OH), carboxylic (COOH) and ester groups, are able to coordinate with the different transition element ions and especially in a bidentate type.

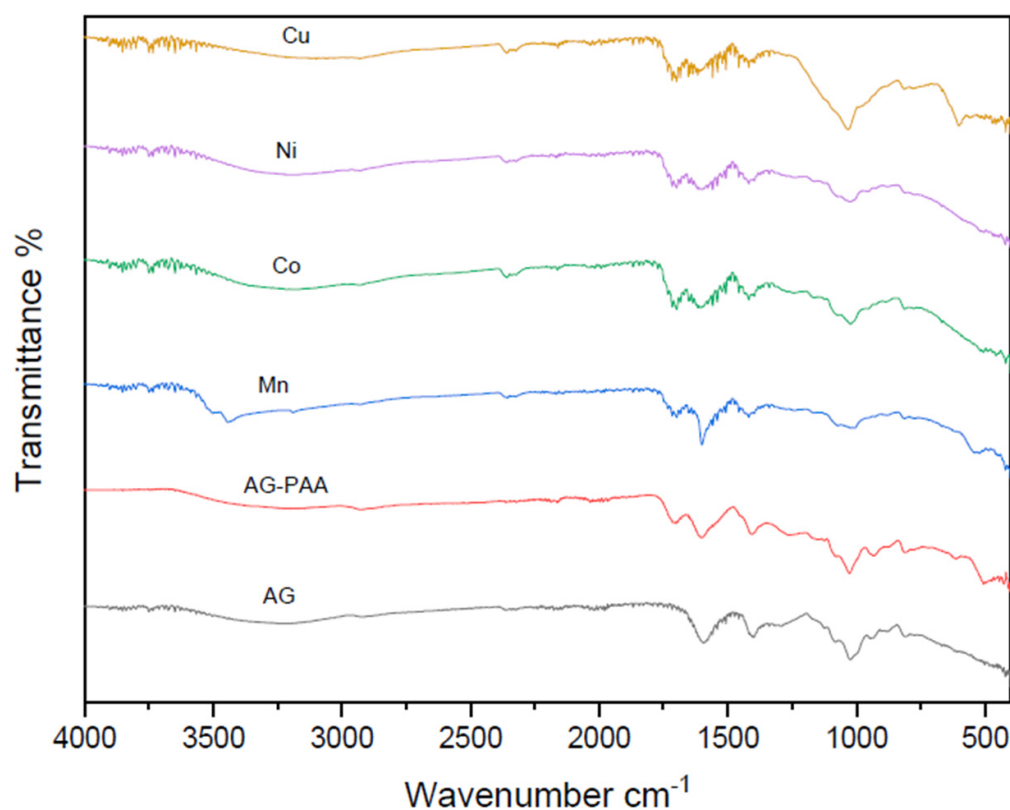


Figure 3. FT-IR spectra of the alginate (AG), polymeric ligand (poly-PAA/AG) and the different synthesized Co(II), Cu(II), Mn(II) and Ni(II) polymeric compounds.

3.4. Electronic Spectra

The electronic spectra of transition metal polymeric and their free ligands (poly-PAA/AG) are measured in the presence of DMSO (10^{-3} M). The outcomes show up in Table 3. The UV-Vis spectrum of (AG) peaks at 254 nm are appropriated to ($\pi \rightarrow \pi^*$) [49]. PAA displayed bands of absorbance at 270 nm appropriated to $n \rightarrow \pi^*$ [50]. As for the electronic spectra of polymeric compounds for cobalt(II), copper(II), manganese(II) and nickel(II), it has special bands, in the visible zone of spectra assigned to d-d transition scopes at 492–580 nm. As for the bands identical to $\pi \rightarrow \pi^*$ and $n \rightarrow \pi^*$, transitions were shown in the scopes of 258–277 nm and 273–298 nm, respectively, which indicates a bonding between the ligand (poly-PAA/AG) and the transition metals. The electronic spectrum of the Mn(II) compound in DMSO solution exhibited a peak around 510 nm assignable to the ${}^6A_{1g} \rightarrow {}^4E_g, {}^4A_{1g}$ transition. These data along with magnetic data are compatible with an octahedral structure around the transition metal ion [51]. The cobalt(II) polymeric complex displayed a weaker broad absorption band at 560 nm appointed to ${}^4T_{1g}(F) \rightarrow {}^4T_{1g}(P)$ transition of octahedral geometry [52]. The nickel(II) polymeric complex showed two bands located at 512 and 580 nm, which may be referred to as ${}^3A_{2g}(F) \rightarrow {}^3T_{1g}(P)(\nu_3)$ and ${}^3A_{2g}(F) \rightarrow {}^3T_{1g}(F)(\nu_2)$, which are characteristic of the nickel(II) ion, in an octahedral geometry [53]. The electronic spectrum of copper(II) showed a low-intensity broad band at 690 nm corresponding to the ${}^2E_g \rightarrow {}^2T_{2g}$ transition, suggesting a distorted octahedral structure around Cu(II) [54].

Table 3. Electronic spectral data of free ligand and its polymeric compounds and magnetic moments.

Ligands and the Complexes	λ_{max} (nm)	$\bar{\nu}$ (cm^{-1})	Assignment	μ_{eff} (B.M.)	Geometry
PAA	270	37,037	$n \rightarrow \pi^*$	-	-
AG	254	39,370	$\pi \rightarrow \pi^*$	-	-
Co(II) complex	560	17,857	${}^4T_{1g}(F) \rightarrow {}^4T_{1g}(P)$	4.82	Octahedral
	273	36,630	$n \rightarrow \pi^*$		
	258	38,759	$\pi \rightarrow \pi^*$		
Cu(II) complex	690	14,490	${}^2E_g \rightarrow {}^2T_{2g}$	1.74	Octahedral
	277	36,101	$n \rightarrow \pi^*$		
	263	38,022	$\pi \rightarrow \pi^*$		
Mn(II) complex	510	19,607	${}^6A_{1g} \rightarrow {}^4E_g, {}^4A_{1g}$	5.94	Octahedral
	278	35,971	$n \rightarrow \pi^*$		
	263	38,022	$\pi \rightarrow \pi^*$		
Ni(II) complex	512	19,531	${}^3A_{2g}(F) \rightarrow {}^3T_{1g}(P)(v_3)$	2.88	Octahedral
	580	17,241	${}^3A_{2g}(F) \rightarrow {}^3T_{1g}(F)(v_2)$		
	286	34,965	$n \rightarrow \pi^*$		
	251	39,840	$\pi \rightarrow \pi^*$		

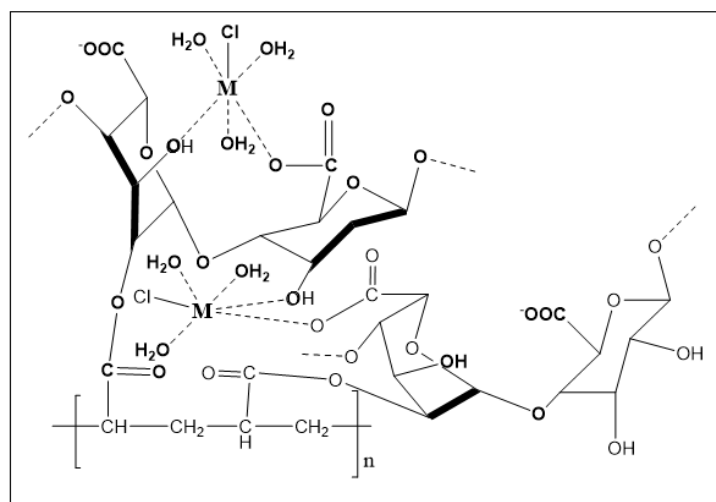
3.5. Magnetic Moment Analysis

The determination of magnetic susceptibilities (μ_{eff}) of the polymeric compounds was carried out at 25 °C. The data of the effective magnetic moment (μ_{eff}) were specified by the data of diamagnetic corrections and Pascal's constants according to Equation (2):

$$\mu_{\text{eff}} = 2828(\chi_{\text{MT}})^{1/2} \text{ (in B.M.)} \quad (2)$$

where μ_{eff} is the effective magnetic moment (in Bohr Magneton, B.M.), T is the temperature (K) and χ_{M} is the molar magnetic susceptibility after correction. The value of μ_{eff} for the Mn(II) complex was 5.94 μB , which suggested an octahedral geometry, whereas, in the case of the Co(II) complex, the magnetic measurements illustrated a 4.82 μB value, which is sufficient for octahedral geometry [55,56]. As for the Ni(II) compound, magnetic measurements revealed that the compound has a μ_{eff} value of 2.88 μB , which is compatible with the range of the expected octahedral geometry of the nickel(II) compound [57]. Moreover, it has been found that the Cu(II) compound stabilizes in an octahedral geometry with a value of 1.74 μB [58].

The suggested structures for nano-sized Co(II), Cu(II), Mn(II) and Ni(II) coordination PAA/alginate biopolymers are shown in Figure 4.

**Figure 4.** Suggested structure of metallic coordination polymers.

Where M = Cobalt(II), copper(II), manganese(II) or nickel(II).

3.6. Thermal Analysis

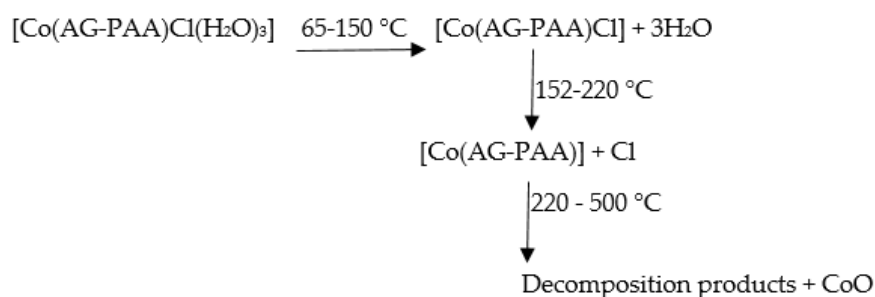
Thermal analyses of the manufactured compounds were performed up to 500 °C. Using this method, complex composition, temperature stability and the presence or absence of water molecules (if any) inside or outside the compounds inner coordination sphere can all be determined. TGA thermograms of the synthesized ligand and transition metal polymeric complexes showed a gradual weight reduction, indicating disintegration by fragmentation as the temperature increased. The findings revealed a good agreement between the calculated data, and the suggested formulae for weight loss (Table 4).

Table 4. Thermal analysis of polymeric complexes.

Compounds	Stage	Temp. Range (°C)	TGA (Wt. Loss) (%)		Assignment
			Found	Calcd.	
Co(II) complex	1st	65–150	13.94	14.32	Loss of three water molecules
	2nd	152–220	9.05	9.38	Loss of chloride atom
	3rd	222–350	59.83	60.94	Decomposition rest of the organic ligand AG-PAA with the formation of cobalt oxide
	4th	352–500			
Cu(II) complex	1st	60–118	13.98	14.15	Loss of three water molecules
	2nd	120–205	9.18	9.27	Loss of chloride atom
	3rd	207–326	59.32	60.20	Decomposition rest of the organic ligand AG-PAA with the formation of copper oxide
	4th	328–500			
Mn(II) complex	1st	70–142	13.90	14.46	Loss of three water molecules
	2nd	144–202	9.12	9.48	Loss of chloride atom
	3rd	204–295	59.88	61.59	Decomposition rest of the organic ligand AG-PAA with the formation of manganese oxide
	4th	297–500			
Ni(II) complex	1st	64–138	13.65	14.31	Loss of three water molecules
	2nd	140–230	9.08	9.39	Loss of chloride atom
	3rd	232–368	59.72	60.98	Decomposition rest of the organic ligand AG-PAA with the formation of nickel oxide
	4th	370–500			

3.6.1. [Co(AG-PAA)Cl(H₂O)₃] Complex

Four decomposition stages were observed for the thermolysis curve of the Co(II) polymeric complex. These occur in the temperature ranges 65–150, 152–220, 222–350 and 352–500 °C. The first mass loss correlates well with the release of three H₂O molecules. This may be referred to as an ion-dipole interaction between cobalt and water. The corresponding mass loss was found to 13.94% (calc. 14.32%). For this step, a DTG midpoint appears at 92 °C with an endothermic peak in the DTA curve, at 94 °C. In the subsequent steps, the decomposition of the complex proceeds. The ultimate product was characterized as cobalt oxide (calc. 19.84%, found 17.18%). Scheme 1 depicts these decompositions.



Scheme 1. Steps for decomposition of Co(II) polymeric complex.

3.6.2. [Cu(AG-PAA)Cl(H₂O)₃] Complex

The TG thermogram of [Cu(AG-PAA)Cl(H₂O)₃] exhibits four inflection points corresponding to four decomposition steps. Three water molecules are released in the first step, (calc. 14.15%, found 13.98%). For this step (thermal gravimetric analysis) (peak at 96 °C), an endothermic effect is observed at 98 °C in the differential thermal analysis trace. The observed mass loss in the 2nd step (120–205 °C) agrees well with the expected loss of chloride atoms (calc. 9.27%, found 9.18%) (DTG peak at 180 °C). This step is marked on the differential thermal analysis (DTA) curve as an exothermic peak at 182 °C. Then, the decomposition products are produced in the rest of the steps. The 3rd and 4th steps are consistent with the decomposition of rest products (calc. 60.20%, found 59.32%) (thermal gravimetric analysis) (peaks at 290 and 386 °C), for which exothermic peaks at 292 and 388 °C are recorded in the DTA trace. The residue was suggested to be CuO on the basis of mass loss consideration (calc. 20.80%, found 17.52%).

3.6.3. [Mn(AG-PAA)Cl(H₂O)₃] Complex

There were four distinct stages of decomposition visible in the Mn(II) complex thermograms. The first stage of decomposition occurs between 70 °C and 142 °C, where the loss of three H₂O molecules results in a rated mass loss of 13.90% (calculated to be 14.46%) (thermal gravimetric analysis TG) (peak at 98 °C), for which a broad, endothermic peak manifests in the DTA curve at 100 °C. In the second stage, chloride atoms are lost with a mass loss of 9.12% percent (calculated as 9.48 percent) between 144 and 202 °C. At this stage, a DTG peak manifests at 182 °C, and a broad endothermic effect is listed in the differential thermal analysis trace at 184 °C. The third and fourth stages of decomposition took place at 204–295 °C and 297–500 °C, respectively, as a result of the remain of the organic ligand AG-PAA decomposing and forming the final product (MnO), which experienced mass losses of 59.88% (calculated at 61.59%) and 17.10% (calculated at 18.98%). These stages are manifested in the DTG curve as peaks at 244 and 384 °C, and the DTA trace furnishes a broad exothermic effect at 246 and 386 °C. (Figure 5).

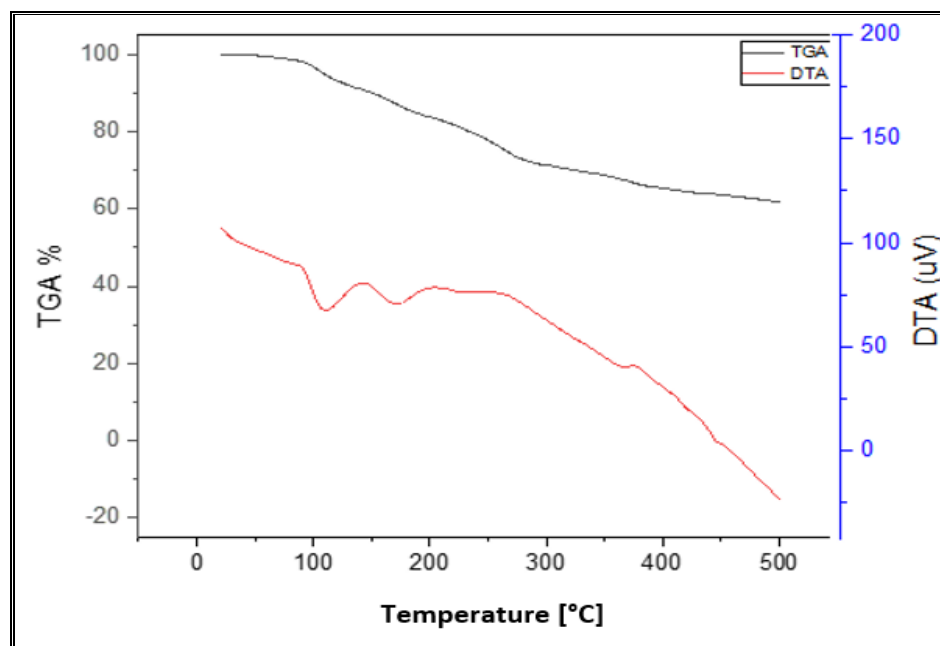


Figure 5. Thermal gravimetric analysis and differential thermal analysis thermograms of Mn(II) compound.

3.6.4. [Ni(AG-PAA)Cl(H₂O)₃] Complex

The decomposition of [Ni(AG-PAA)Cl(H₂O)₃] proceeds in four distinct steps in the temperature ranges 64–138, 140–230, 232–368 and 370–500 °C. The 1st mass loss correlates well with the relief of three H₂O molecules (calc. 14.31%, found 13.65%) (thermal gravimetric analysis) (peak at 98 °C) with an endothermic broad peak in the differential thermal analysis trace at 100 °C. The second mass loss is compatible with the expulsion of the chloride atom (calc. 9.39%, found 9.08%), A thermal gravimetric analysis peak at 202 °C and an exothermic effect at 204 °C in the differential thermal analysis trace are noticed. The third and fourth mass loss represents the release of the rest of organic (AG-PAA) ligands (calc. 60.98%, found 59.72%). The final product is consistent with NiO (calc. 19.79%, found 17.55%).

3.7. X-ray Powder Diffraction

This XRD study is another piece of proof for the emergence of metal–ligand complexes. The compounds' XRD patterns were documented. Table 5 lists the crystal structures of various compounds. The comparison of the diffraction patterns of the ligands with the obtained complexes.

Table 5. X-ray powder diffraction data of the different polymeric compounds (Cu-K α radiation ($\lambda_{Cu} = 0.154059 \text{ \AA}$)).

Parameters	Crosslinked Polymeric Ligand (Poly-PAA/AG)	Co(II) Complex	Cu(II) Complex	Mn(II) Complex	Ni(II) Complex
Empirical formula	C ₉ H ₁₀ O ₇	C ₉ H ₁₅ CoClO ₁₀	C ₉ H ₁₅ CuClO ₁₀	C ₉ H ₁₅ MnClO ₁₀	C ₉ H ₁₅ NiClO ₁₀
Formula Weight	230.12	377.60	382.21	373.60	377.36
a (Å)	20.22	7.967	7.8447	7.4014	5.673
b (Å)	11.58	7.967	7.8447	8.7901	5.655
c (Å)	20.74	7.967	26.358	3.6889	8.004
Alfa (°)	90.00	90.00	90.00	90.00	90.35
Beta (°)	110.64	90.00	90.00	98.165	90.72
gamma (°)	90.00	90.00	120.00	90.00	89.99
Crystal system	Monoclinic	Cubic	Hexagonal	Monoclinic	Triclinic
Space group	C12/m1	Fm-3m	R-3m	C2/m	I-1
Volume of unit cell (Å ³)	4498	505.8	1404.7	237.57	256.7
Particle size (nm)	171	14	38	33	68

The XRD diffractogram of the ligand film indicates the presence of an amorphous structure, while the prepared Co(II), Cu(II), Mn(II) and Ni(II) compounds were crystalline. All polymeric complexes have sharp peaks in Figure 6. On the other hand, the Mn(II) compound has a monoclinic crystal system while the Co(II) compound has a cubic crystal system. The Ni(II) and Cu(II) compounds have a triclinic, and a hexagonal crystal system, respectively. The significant broadening of the peaks illustrates that the particles are of nm dimensions. Scherrer's Equation (3) was used to estimate the particle size of the polymeric complexes.

$$D = K\lambda / \beta \cos\theta \quad (3)$$

where K is the shape factor, λ is the X-ray wavelength typically 1.54 Å, β is the line broadening at half the maximum intensity in radians and θ is Bragg angle. D is the mean size of the ordered (crystalline) domains, which may be smaller or equal to the grain size. Scherrer's equation is limited to nanoscale particles. The average size of the particles lies in the range of 14–68 nm which is in agreement with that noticed by scanning electron microscopy.

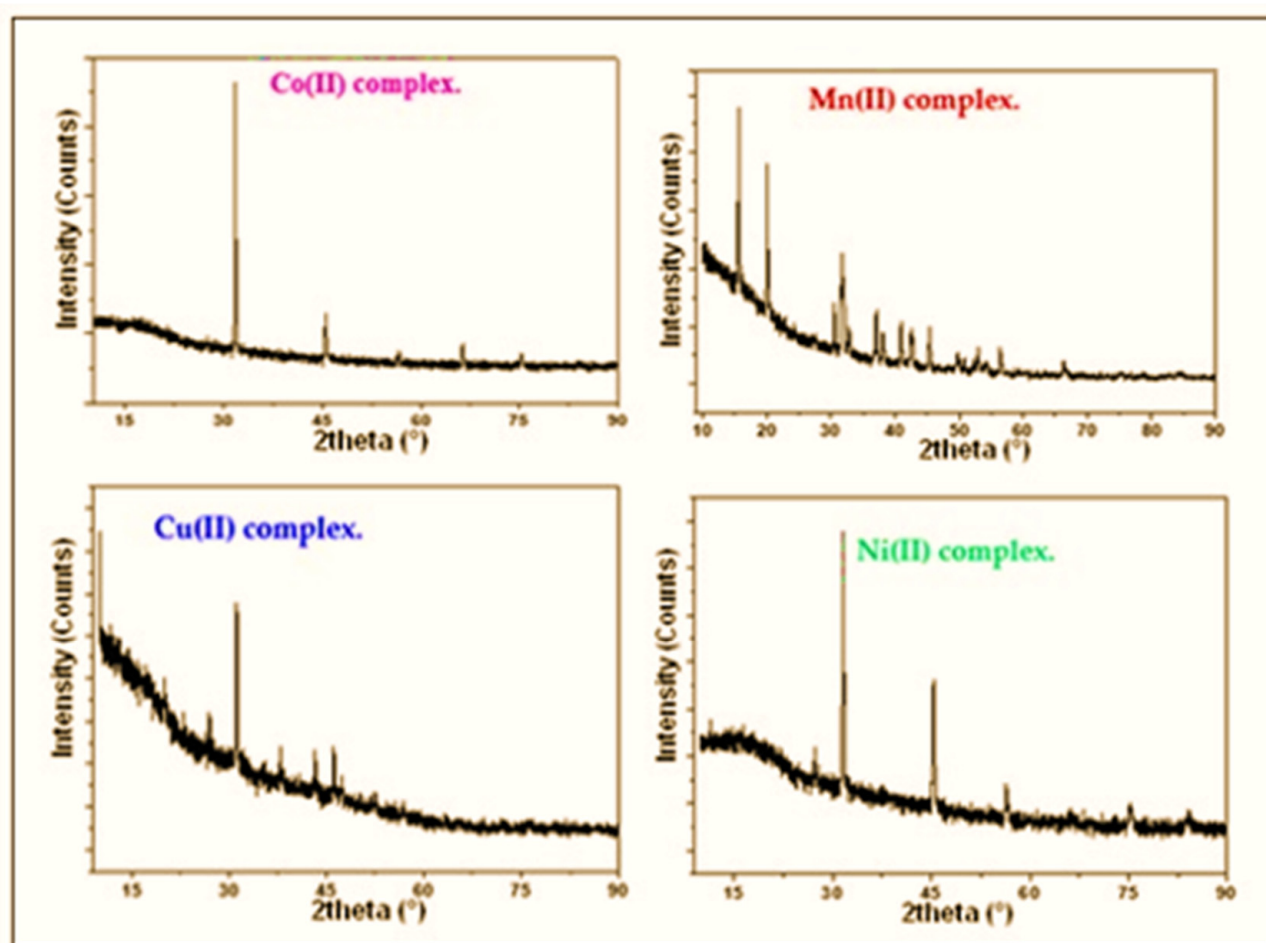


Figure 6. X-ray diffraction patterns of the different synthesized polymeric complexes (Cu-K α radiation ($\lambda_{Cu} = 0.154059 \text{ \AA}$)).

3.8. SEM Morphological Analysis

Electron microscopy (EM) has played a vital function in polymeric complexes properties and analysis. In addition to extremely more magnification levels, it can provide us with significant information containing composition and novel materials' morphology. It can also show distinguishing contaminant materials that are only existent in polymers in trace amounts. Figure 7 displays as a general note an evident difference in surface morphology which is diverse depending on the type of transition element used in prepared polymeric complexes. The crosslinked polymeric ligand (poly-PAA/AG) revealed a porous and irregular surface reflecting its considerable hydrophilic property. This surface property could be efficient in the fashioning of ligand (poly-PAA/AG-metal coordination) polymers, and given that polymeric complexes are readily available in solution, continuous crosslinking into nanostructures is expected. While such particles have been used in the biomedical industry [59], their presence does support the aim to synthesize homogenous Co(II), Cu(II), Mn(II) and Ni(II) coordination PAA/alginate biopolymer NPs. A microscopic image of Mn(II) and Co(II) polymeric compounds illustrates small particles with a diameter between 20 and 29 nm. The surface morphology of the Ni(II) compound appears as uniform spherical particles with a diameter between 60 and 65 nm. In the Cu(II) complex, the SEM shows different shapes with diameters between 34 and 40 nm.

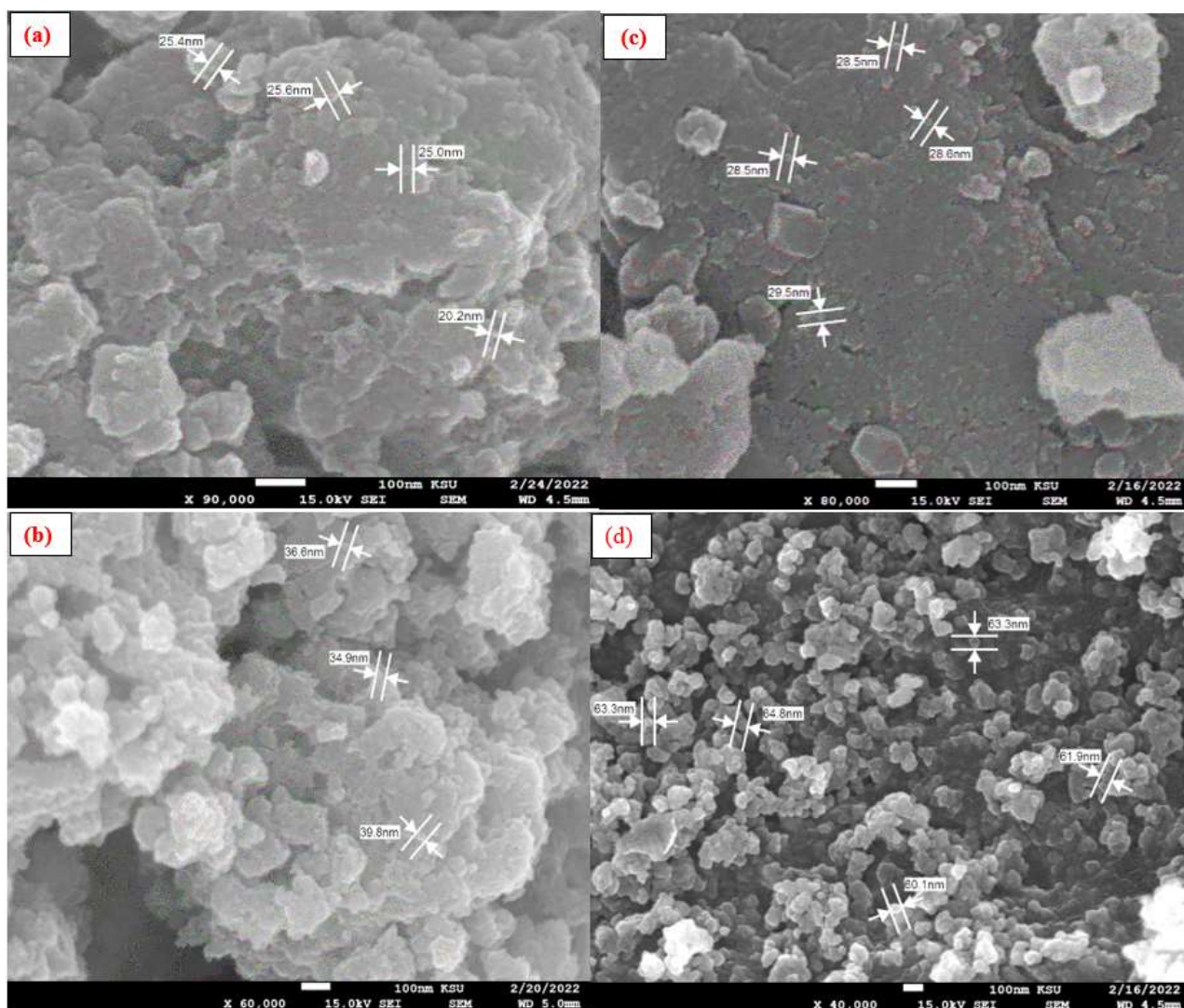


Figure 7. SEM of the different prepared polymeric complexes, (a) Co(II) complex, (b) Cu(II) complex, (c) Mn(II) complex and (d) Ni(II) complex.

3.9. Antimicrobial and Antioxidant Assays

The test polymeric complex NPs exhibit a broad spectrum of antimicrobial activity because they are active against both Gram-positive and Gram-negative bacteria, but especially against Gram-positive strains, according to the antimicrobial results summarized in Table 6 and Figure 8a–d. The inhibitory zone diameter of the other extracts reached 5 cm, demonstrating their strong antimicrobial activity. The strongest are copper(II) and cobalt(II) compounds, which have a strain-dependent antimicrobial effect. The antioxidant effect of the different polymeric complexes is displayed in Figure 9.

Table 6. Antimicrobial and antioxidant effect (Inhibitory zone expressed in cm \pm SD).

Compound	Antimicrobial					Antioxidant
	S1	S4	S5	S10	9C	
Co(II) complex	2.1	1.3	2.2	1.4	3.1	71 \pm 1.4
Cu(II) complex	5.4	1.4	1.7	2.9	4.1	82 \pm 1.4
Mn(II) complex	1	1.65	1.4	1.4	1.3	61 \pm 0.6
Ni(II) complex	1.9	1.3	1.9	1.2	1.35	70.5 \pm 0.7

SD: Standard Deviation.

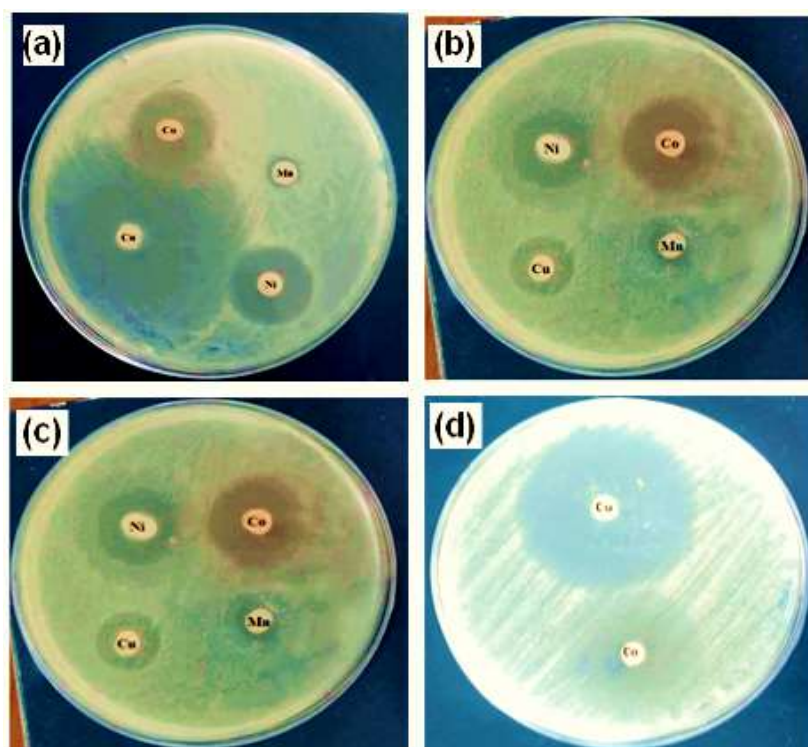


Figure 8. Microbiological activity against (a) *Staphylococcus aureus*, (b) *Escherichia coli*, (c) *Salmonella typhimurium* and (d) *Candida albicans*.

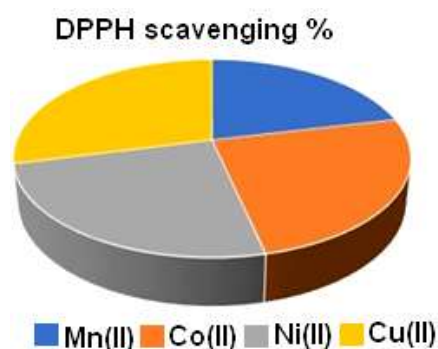


Figure 9. Antioxidant effect of the different polymeric complexes.

3.10. In Vitro Anticancer Assay

In vitro, cell assays proceeded to investigate both the biocompatibility and anticancer activity of the prepared polymeric compounds. Human breast cancer cells (MCF-7) were used to assess the anticancer potential of the crosslinked polysaccharide ligand (poly-AG/PAA) and its two metal coordination polymers, the poly-AG/PAA/copper(II) and the poly-AG/PAA/cobalt(II). The assessment of the anticancer activity was carried out via the treatment of the cancer cells using the MTT assay by varying the concentration of the different polymeric vectors. The outcomes in Figure 10 displayed no cytotoxicity of the polymeric ligand in the approach with normal epithelial cells. This was reported previously by various research investigations that showed the excellent biocompatibility of the naturally extracted polysaccharides [60,61]. Therefore, the crosslinked polymeric ligand based on alginate biopolymer can be considered as a safe drug delivery carrier and other pharmaceutical applications. In addition, the synthesized polymeric compounds of Cu(II) and Co(II) revealed excellent cytocompatibility after 72 h in contact with the normal human breast epithelial cells(MCF10A), with the various applied concentrations. This was an important stage; meanwhile, the potential of anticancer drugs significantly concentrated

on their biocompatibility with the normal counterparts of the analyzed cancer cells. The anticancer valuation in Figure 11 exhibited that the polymeric ligand without metals has the ability to kill cancer cells, and this is from a dose of 50 $\mu\text{g/mL}$. The anticancer performance increases by sample concentration, to reach 51% at a concentration of 200 $\mu\text{g/mL}$, which is in concordance with some previous studies [62].

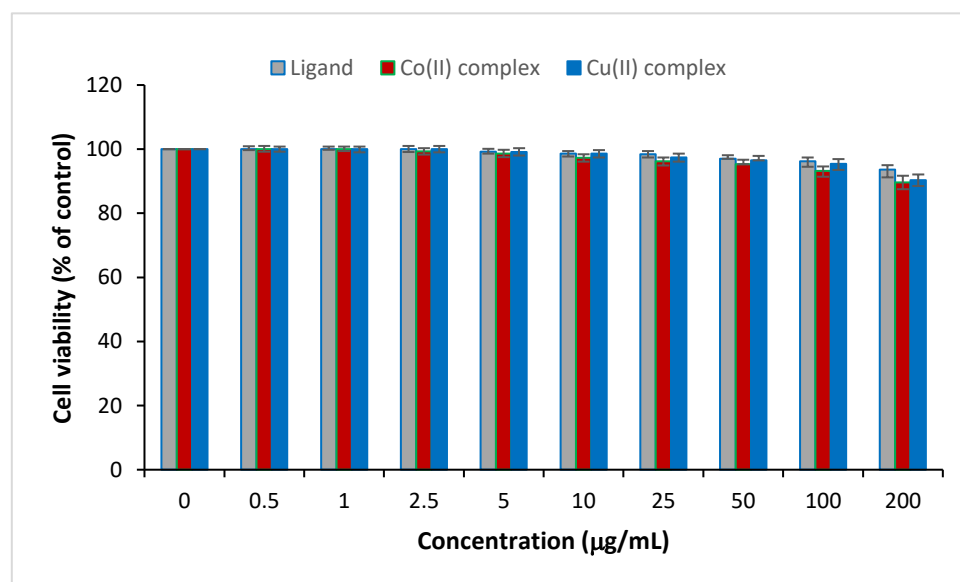


Figure 10. Cell viability assessments in human normal breast cells of the ligand and the polymeric compounds via cell growth inhibition rates by varying the concentration after 72 h incubation on MCF-10A and MCF-7 cell lines.

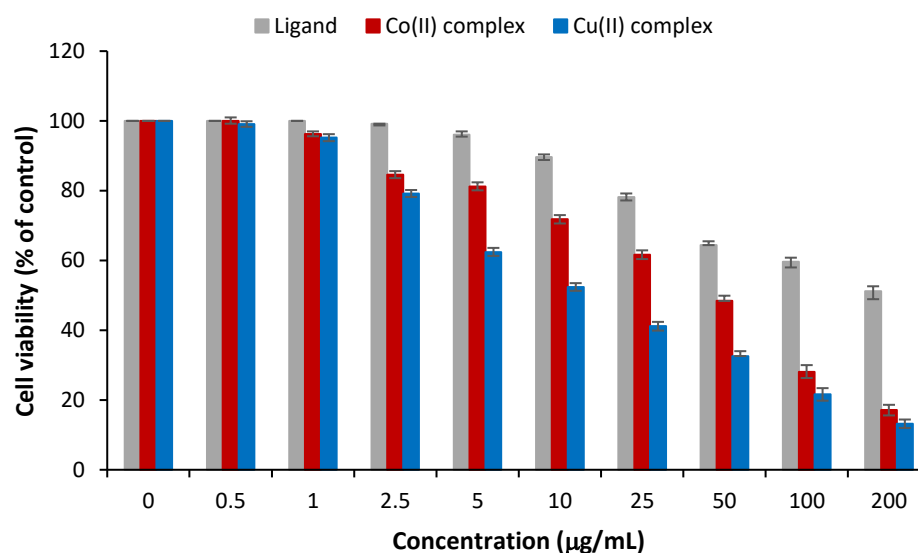


Figure 11. Anticancer activity in human breast cancer cells of the ligand and the polymeric compounds via cell growth inhibition rates by varying the concentration after 72 h incubation on MCF-10A and MCF-7 cell lines.

Concerning the two selected polymeric complexes, results showed a good ability to kill the cancer cells in a dose-dependent method. The copper(II) polymeric compound confirms its excellent performance shown in microbial activity and demonstrates a higher anticancer potential compared to the Co(II) complex with the different polymeric doses. After a period of incubation fixed at 72 h and at a dose of 200 $\mu\text{g/mL}$, the transition metal complexation significantly lowered the viability of the MCF-7 cancer cells up to $17.1 \pm 1.21\%$

and $13.2 \pm 1.52\%$ for the copper(II) and the cobalt(II) polymeric compounds, respectively. In summary, both the polymeric ligand (poly-AG/PAA) and the Cu(II) and Co(II) compounds exhibited good cytocompatibility with normal human epithelial cells. Furthermore, the in vitro anticancer evaluation showed the high anticancer performance of the Cu(II) and Co(II) polymeric compounds with a potential rising with the used polymeric concentration.

4. Conclusions

Polymeric complex NPs were prepared from polyacrylic acid (PAA) and sodium alginate (AG) with cobalt(II), copper(II), manganese(II) and nickel(II) chlorides. The various physico-chemical analyses included elemental analysis (C and H), FT-IR, UV-Vis spectra, TG, DTA, XRD and SEM. The magnetic studies suggested the octahedral geometrical structure for all produced polymeric complexes. Alginate and polyacrylic acid were used because they are biocompatible materials. As it is known, (PAA) gels are suitable biocompatible matrices for medical applications, such as gels for skin care products. PAA films can be deposited on orthopedic implants to protect them from corrosion. Crosslinked hydrogels of PAA and gelatin have also been used as in medical glue. In addition, Alginate (AG), which is rich in sources, is non-toxic and has excellent biocompatibility, biodegradability and safety, has been widely used in medical wound dressings, drug delivery carriers and delivery of bioactive substances in tissue engineering and skeleton materials. Therefore, nano-sized metallic polymers were prepared from these biopolymers, which really gave excellent results with the microbes that were tested, whether Gram-positive or Gram-negative bacteria or fungi. In summary, both the polymeric ligand (poly-AG/PAA) and the two metal complexes exhibited good cytocompatibility with normal human epithelial cells. Furthermore, the in vitro anticancer evaluation showed the high anticancer performance of the poly-AG/PAA/Cu(II) and poly-AG/PAA/Co(II) compounds with a potential rise with the used polymeric concentration.

Author Contributions: Data curation, M.S.A.-F., M.S.A. and Y.E.-G.; formal analysis, M.S.A.-F., M.S.A. and Y.E.-G.; investigation, M.S.A.-F., M.S.A. and Y.E.-G.; methodology, M.S.A.-F. and Y.E.-G.; project administration, M.S.A.-F.; software, M.S.A.-F. and M.S.A.; supervision, M.S.A.-F. and Y.E.-G.; validation, M.S.A.-F. and Y.E.-G.; writing—original draft, M.S.A.-F. and M.S.A.; writing—review and editing, M.S.A.-F. All authors have read and agreed to the published version of the manuscript.

Funding: This research received no external funding.

Data Availability Statement: The data are contained within the article.

Conflicts of Interest: The authors declare no conflict of interest.

References

1. Ezeoha, S.L. Production of Biodegradable Plastic Packaging Film from Cassava Starch. *IOSR J. Eng.* **2013**, *3*, 14–20. [[CrossRef](#)]
2. Rebelo, R.; Fernandes, M.; Figueiro, R. Biopolymers in medical implants: A brief review. *Procedia Eng.* **2017**, *200*, 236–243. [[CrossRef](#)]
3. Bala, I.A.; Abdullahi, M.R.; Bashir, S.S. A review on formulation of enzymatic solution for biopolymer hydrolysis. *J. Chem.* **2017**, *6*, 9–13.
4. Pattanashetti, N.A.; Heggannavar, G.B.; Kariduraganavar, M.Y. Smart biopolymers and their biomedical applications. *Procedia Manuf.* **2017**, *12*, 263–279. [[CrossRef](#)]
5. Qasim, U.; Osman, A.I.; Al-Muhtaseb, A.H.; Farrell, C.; Al-Abri, M.; Ali, M.; Vo, D.V.N.; Jamil, F.; Rooney, D.W. Renewable cellulosic nanocomposites for food packaging to avoid fossil fuel plastic pollution: A review. *Environ. Chem. Lett.* **2021**, *19*, 613–641. [[CrossRef](#)]
6. Nessi, V.; Falourd, X.; Maignet, J.-E.; Cahier, K.; D'Orlando, A.; Descamps, N.; Gaucher, V.; Chevigny, C.; Lourdin, D. Cellulose nanocrystals-starch nanocomposites produced by extrusion: Structure and behavior in physiological conditions. *Carbohydr. Polym.* **2019**, *225*, 115123. [[CrossRef](#)]
7. Barclay, T.G.; Day, C.M.; Petrovsky, N.; Garg, S. Review of polysaccharide particle-based functional drug delivery. *Carbohydr. Polym.* **2019**, *221*, 94–112. [[CrossRef](#)]
8. Reis, A.V.; Guilherme, M.R.; Cavalcanti, O.A.; Rubira, A.F.; Muniz, E.C. Synthesis and characterization of pH-responsive hydrogels based on chemically modified Arabic gum polysaccharide. *Polymer* **2006**, *47*, 2023–2029. [[CrossRef](#)]

9. Farooqi, Z.U.R.; Qadeer, A.; Hussain, M.M.; Zeeshan, N.; Ilic, P. Characterization and physicochemical properties of nanomaterials. In *Nanomaterials: Synthesis, Characterization, Hazards and Safety*; Elsevier: Amsterdam, The Netherlands, 2021; pp. 97–121. [[CrossRef](#)]
10. Salem, S.S.; Fouda, A. Green Synthesis of Metallic Nanoparticles and Their Prospective Biotechnological Applications: An Overview. *Biol. Trace Elem. Res.* **2021**, *199*, 344–370. [[CrossRef](#)]
11. Nikalje, A.P. Nanotechnology and its applications in medicine. *Med. Chem.* **2015**, *5*, 081–089. [[CrossRef](#)]
12. Barik, T.K.; Maity, G.C.; Gupta, P.; Mohan, L.; Santra, T.S. Nanomaterials: An Introduction. *Nanomater. Their Biomed. Appl.* **2021**, *16*, 1–11.
13. Singh, B.K.; Lee, S.; Na, K. An overview on metal-related catalysts: Metal oxides, nanoporous metals and supported metal nanoparticles on metal organic frameworks and zeolites. *Rare Metals* **2020**, *39*, 751–766. [[CrossRef](#)]
14. Salem, S.S.; Fouda, M.M.G.; Fouda, A.; Awad, M.A.; Al-Olayan, E.M.; Allam, A.A.; Shaheen, T.I. Antibacterial, Cytotoxicity and Larvicidal Activity of Green Synthesized Selenium Nanoparticles Using *Penicillium corylophilum*. *J. Clust. Sci.* **2021**, *32*, 351–361. [[CrossRef](#)]
15. Khan, S.; Mansoor, S.; Rafi, Z.; Kumari, B.; Shoaib, A.; Saeed, M.; Alshehri, S.; Ghoneim, M.M.; Rahamathulla, M.; Hani, U.; et al. A review on nanotechnology: Properties, applications, and mechanistic insights of cellular uptake mechanisms. *J. Mol. Liquids* **2021**, *347*, 118008. [[CrossRef](#)]
16. Pérez-Hernández, H.; Pérez-Moreno, A.; Sarabia-Castillo, C.; García-Mayagoitia, S.; Medina-Pérez, G.; López-Valdez, F.; Campos-Montiel, R.; Jayanta-Kumar, P.; Fernández-Luqueño, F. Ecological Drawbacks of Nanomaterials Produced on an Industrial Scale: Collateral Effect on Human and Environmental Health. *Water Air Soil Pollut.* **2021**, *232*, 435. [[CrossRef](#)] [[PubMed](#)]
17. Singh, R.; Singh, S. Nanomanipulation of consumer goods: Effects on human health and environment. In *Nanotechnology in Modern Animal Biotechnology*; Springer: Berlin/Heidelberg, Germany, 2019; pp. 221–254. [[CrossRef](#)]
18. Pathakoti, K.; Goodla, L.; Manubolu, M.; Hwang, H.-M. Nanoparticles and Their Potential Applications in Agriculture, Biological Therapies, Food, Biomedical, and Pharmaceutical Industry: A Review. In *Nanotechnology and Nanomaterial Applications in Food, Health, and Biomedical Sciences*; Apple Academic Press: Palm Bay, FL, USA, 2019; pp. 121–162. ISBN 9780429425660.
19. Elkodous, M.A.; El-Husseiny, H.M.; El-Sayyad, G.S.; Hashem, A.H.; Doghish, A.S.; Elfadil, D.; Radwan, Y.; El-Zeiny, H.M.; Bedair, H.; Ikhdair, O.A.; et al. Recent advances in waste-recycled nanomaterials for biomedical applications: Waste-to-wealth. *Nanotechnol. Rev.* **2021**, *10*, 1662–1739. [[CrossRef](#)]
20. Parker, G. Measuring the environmental performance of food packaging: Life cycle assessment. In *Environmentally Compatible Food Packaging*; Elsevier: Amsterdam, The Netherlands, 2008; pp. 211–237.
21. Shankar, S.; Rhim, J.-W. Bionanocomposite films for food packaging applications. In *Reference Module in Food Science*; Elsevier: Amsterdam, The Netherlands, 2018; pp. 1–10.
22. Hassan, M.E.; Bai, J.; Dou, D.Q. Biopolymers; Definition, classification and applications. *Egypt. J. Chem.* **2019**, *62*, 1725–1737. [[CrossRef](#)]
23. Soldo, A.; Miletić, M.; Auad, M.L. Biopolymers as a sustainable solution for the enhancement of soil mechanical properties. *Sci. Rep.* **2020**, *10*, 267. [[CrossRef](#)]
24. Song, J.; Winkeljann, B.; Lieleg, O. Biopolymer-based coatings: Promising strategies to improve the biocompatibility and functionality of materials used in biomedical engineering. *Adv. Mater. Interfaces* **2020**, *7*, 2000850. [[CrossRef](#)]
25. Jummaat, F.; Yahya, E.B.; Khalil H.P.S., A.; Adnan, A.S.; Alqadhi, A.M.; Abdullah, C.K.; A.K., A.S.; Olaiya, N.G.; Abdat, M. The Role of Biopolymer-Based Materials in Obstetrics and Gynecology Applications: A Review. *Polymers* **2021**, *13*, 633. [[CrossRef](#)] [[PubMed](#)]
26. Reddy, M.S.B.; Ponnamma, D.; Choudhary, R.; Sadasivuni, K.K. A Comparative Review of Natural and Synthetic Biopolymer Composite Scaffolds. *Polymers* **2021**, *13*, 1105. [[CrossRef](#)]
27. Olivia, M.; Jingga, H.; Toni, N.; Wibisono, G. Biopolymers to improve physical properties and leaching characteristics of mortar and concrete: A review. In *IOP Conference Series: Materials Science and Engineering*; Institute of Physics Publishing: Bristol, UK, 2018; Volume 345, p. 012028.
28. Darge, H.F.; Andrgie, A.T.; Tsai, H.C.; Lai, J.Y. Polysaccharide and polypeptide based injectable thermo-sensitive hydrogels for local biomedical applications. *Int. J. Biol. Macromol.* **2019**, *133*, 545–563. [[CrossRef](#)]
29. Mohammed, A.S.A.; Naveed, M.; Jost, N. Polysaccharides; classification, chemical properties, and future perspective applications in fields of pharmacology and biological medicine (a review of current applications and upcoming potentialities). *J. Polym. Environ.* **2021**, *29*, 2359–2371. [[CrossRef](#)]
30. Grasdalen, H.; Larsen, B.; Smidsrød, O. ¹³C-NMR studies of alginate. *Carbohydr. Res.* **1977**, *56*, C11–C15. [[CrossRef](#)]
31. Grasdalen, H.; Larsen, B.; Smidsrød, O. A pmr study of the composition and sequence of uronate residues in alginates. *Carbohydr. Res.* **1979**, *68*, 23–31. [[CrossRef](#)]
32. Kothale, D.; Verma, U.; Dewangan, N.; Jana, P.; Jain, A.; Jain, D. Alginate as Promising Natural Polymer for Pharmaceutical, Food, and Biomedical Applications. *Curr. Drug Deliv.* **2020**, *17*, 755–775. [[CrossRef](#)]
33. EL-Ghoul, Y.; Al-Fakeh, M.S.; Al-Subai, N. Synthesis and Characterization of a New Alginate/Carrageenan crosslinked biopolymer and Study of the Antibacterial, Antioxidant, and Anticancer Performance of its Mn(II), Fe(III), Ni(II), and Cu(II) polymeric complexes. *Polymers* **2023**, *15*, 2511. [[CrossRef](#)]

34. da Silva, T.L.; Vidart, J.M.M.; da Silva, M.G.C.; Gimenes, M.L.; Vieira, M.G.A. Alginate and sericin: Environmental and pharmaceutical applications. *Biol. Act. Appl. Mar. Polysacch.* **2017**, *57*–86. [[CrossRef](#)]
35. Draget, K.I.; Taylor, C. Chemical, physical and biological properties of alginates and their biomedical implications. *Food Hydrocolloids* **2011**, *25*, 251–256. [[CrossRef](#)]
36. Gheorghita Puscaselu, R.; Lobiuc, A.; Dimian, M.; Covasa, M. Alginate: From food industry to biomedical applications and management of metabolic disorders. *Polymers* **2020**, *12*, 2417. [[CrossRef](#)]
37. Orwoll, R.A.; Chong, Y.S. Poly(acrylic acid). In *Polymer Data Handbook*; James, M., Ed.; Oxford University Press: Oxford, UK, 1999; pp. 252–253.
38. Zhuo, W. *Synthesis, Characterization, and Self-Assembly of Amphiphilic Copolymer Based on Poly (Acrylic Acid)*; National University of Singapore: Singapore, 2015.
39. Arkaban, H.; Barani, M.; Akbarizadeh, M.R.; Pal Singh Chauhan, N.; Jadoun, S.; Dehghani Soltani, M.; Zarrintaj, P. Polyacrylic Acid Nanoplatfoms: Antimicrobial, Tissue Engineering, and Cancer Theranostic Applications. *Polymers* **2022**, *14*, 1259. [[CrossRef](#)] [[PubMed](#)]
40. Xu, M.; Zhu, J.; Wang, F.; Xiong, Y.; Wu, Y.; Wang, Q.; Weng, J.; Zhang, Z.; Chen, W.; Liu, S. Improved in vitro and in vivo biocompatibility of graphene oxide through surface modification: Poly (acrylic acid)-functionalization is superior to PEGylation. *ACS Nano* **2016**, *10*, 3267–3281. [[CrossRef](#)] [[PubMed](#)]
41. Mahon, R.; Balogun, Y.; Oluyemi, G.; Njuguna, J. Swelling performance of sodium polyacrylate and poly(acrylamide-co-acrylic acid) potassium salt. *SN Appl. Sci.* **2020**, *2*, 117–132. [[CrossRef](#)]
42. Dumitraşcu, A.-M.; Caras, I.; Ţucureanu, C.; Ermeneanu, A.-L.; Tofan, V.-C. Nickel (II) and Cobalt (II) Alginate Biopolymers as a “Carry and Release” Platform for Polyhistidine-Tagged Proteins. *Gels* **2022**, *8*, 66. [[CrossRef](#)] [[PubMed](#)]
43. Sharafshadeh, M.S.; Tafvizi, F.; Khodarahmi, P.; Ehtesham, S. Preparation and physicochemical properties of cisplatin and doxorubicin encapsulated by niosome alginate nanocarrier for cancer therapy. *Int. J. Biol. Macromol.* **2023**, *235*, 123686. [[CrossRef](#)]
44. Mahdhi, A.; Leban, N.; Chakroun, I.; Chaouch, M.A.; Hafsa, J.; Fdhila, K.; Mahdouani, K.; Majdoub, H. Extracellular polysaccharide derived from potential probiotic strain with antioxidant and antibacterial activities as a prebiotic agent to control pathogenic bacterial biofilm formation. *Microb. Pathogenesis* **2017**, *109*, 214–220. [[CrossRef](#)]
45. Ammar, C.; Alminderej, F.M.; EL-Ghoul, Y.; Jabli, M.; Shafiquzzaman, M. Preparation and Characterization of a New Polymeric Multi-Layered Material Based K-Carrageenan and Alginate for Efficient Bio-Sorption of Methylene Blue Dye. *Polymers* **2021**, *13*, 411. [[CrossRef](#)]
46. Deacon, G.B.; Phillips, R.J. Relationships between the carbon-oxygen stretching frequencies of carboxylato complexes and the type of carboxylate coordination. *Coord. Chem. Rev.* **1980**, *33*, 227–250. [[CrossRef](#)]
47. Al-Fakeh, M.S.; Alsikhan, M.A.; Alnawmasi, J.S. Physico-Chemical Study of Mn(II), Co(II), Cu(II), Cr(III), and Pd(II) Complexes with Schiff-Base and Aminopyrimidyl Derivatives and Anti-Cancer, Antioxidant, Antimicrobial Applications. *Molecules* **2023**, *28*, 2555. [[CrossRef](#)]
48. Al-Fakeh, M.S.; Messaoudi, S.; Alresheedi, F.I.; Albadri, A.E.; El-Sayed, W.A.; Saleh, E.E. Preparation, Characterization, DFT Calculations, Antibacterial and Molecular Docking Study of Co(II), Cu(II), and Zn(II) Mixed Ligand Complexes. *Crystals* **2023**, *13*, 118. [[CrossRef](#)]
49. Yue, W.; Zhang, H.H.; Yang, Z.N.; Xie, Y. Preparation of low-molecular-weight sodium alginate by ozonation. *Carbohydr. Polym.* **2021**, *251*, 117104. [[CrossRef](#)] [[PubMed](#)]
50. Vetriselvi, V.; Santhi Raj, R.J.J. Synthesis and characterization of poly acrylic acid modified with dihydroxy benzene-redox polymer. *Res. J. Chem. Sci.* **2014**, *4*, 78–86.
51. Parihari, R.K.; Patel, R.K.; Patel, R.N. Synthesis and characterization of metal complexes of manganese-, cobalt-and zinc (II) with Schiff base and some neutral ligand. *J. Indian Chem. Soc.* **2000**, *77*, 339.
52. Mohanan, K.; Murukan, B. Complexes of manganese (II), iron (II), cobalt (II), nickel (II), copper (II), and zinc (II) with a bishydrazone. *Synth. React. Inorg. Met. Org. Nano Met. Chemistry* **2005**, *35*, 837–844. [[CrossRef](#)]
53. Gupta, L.K.; Bansal, U.; Chandra, S. Spectroscopic and physicochemical studies on nickel(II) complexes of isatin-3,2'-quinolyhydrazones and their adducts. *Spectrochim. Acta Part A Mol. Biomol. Spectro.* **2007**, *66*, 972–975. [[CrossRef](#)]
54. Ajaykumar, D. Kulkarni, et, Synthesis, spectral, electrochemical and biological studies of Co(II), Ni(II) and Cu(II) complexes with Schiff bases of 8-formyl-7-hydroxy-4-methyl coumarin. *J. Coord. Chem.* **2009**, *62*, 481–492.
55. Al-Fakeh, M.S.; Allazzam, G.A.; Yarkandi, N.H. Ni (II), Cu (II), Mn (II), and Fe (II) Metal Complexes Containing 1, 3-Bis (diphenylphosphino) propane and Pyridine Derivative: Synthesis, Characterization, and Antimicrobial Activity. *Int. J. Biomater.* **2021**, *2021*, 4981367. [[CrossRef](#)]
56. Al-Fakeh, M.S.; Alsaedi, R.O. Synthesis, characterization, and antimicrobial activity of CoO nanoparticles from a Co (II) complex derived from polyvinyl alcohol and aminobenzoic acid derivative. *Sci. World J.* **2021**, *2021*, 6625216. [[CrossRef](#)]
57. Al-Fakeh, M.S. Synthesis, characterization and anticancer activity of NiO nanoparticles from a Ni (II) complex derived from chitosan and pyridine derivative. *Bulg. Chem. Commun.* **2021**, *53*, 321–326.
58. Al-Fakeh, M.S. Synthesis, thermal stability and kinetic studies of copper (II) and cobalt (II) complexes derived from 4-aminobenzohydrazide and 2-mercaptobenzothiazole. *Eur. Chem. Bulletin* **2020**, *9*, 403–409. [[CrossRef](#)]
59. Zhang, H.; Cheng, J.; Ao, Q. Preparation of Alginate-Based Biomaterials and Their Applications in Biomedicine. *Mar. Drugs* **2021**, *19*, 264. [[CrossRef](#)] [[PubMed](#)]

60. Geetha Bai, R.; Tuvikene, R. Potential Antiviral Properties of Industrially Important Marine Algal Polysaccharides and Their Significance in Fighting a Future Viral Pandemic. *Viruses* **2021**, *13*, 1817. [[CrossRef](#)] [[PubMed](#)]
61. Liu, C.; Jiang, F.; Xing, Z.; Fan, L.; Li, Y.; Wang, S.; Ling, J.; Ouyang, X.-K. Efficient Delivery of Curcumin by Alginate Oligosaccharide Coated Aminated Mesoporous Silica Nanoparticles and In Vitro Anticancer Activity against Colon Cancer Cells. *Pharmaceutics* **2022**, *14*, 1166. [[CrossRef](#)] [[PubMed](#)]
62. Gutiérrez-Rodríguez, A.G.; Juárez-Portilla, C.; Olivares-Bañuelos, T.; Zepeda, R.C. Anticancer activity of seaweeds. *Drug Discov. Today* **2018**, *23*, 434–447. [[CrossRef](#)]

Disclaimer/Publisher's Note: The statements, opinions and data contained in all publications are solely those of the individual author(s) and contributor(s) and not of MDPI and/or the editor(s). MDPI and/or the editor(s) disclaim responsibility for any injury to people or property resulting from any ideas, methods, instructions or products referred to in the content.